Geophys. J. Int. (2006) **164,** 149–159 doi: 10.1111/j.1365-246X.2005.02831.x

Attenuation of seismic waves in methane gas hydrate-bearing sand

Jeffrey A. Priest,[1,2] Angus I. Best[1] and Christopher R. I. Clayton[2]

[1]*National Oceanography Centre, Southampton, University of Southampton, Waterfront Campus, European Way, Southampton,* SO14 3ZH, *UK. E-mail: J.A.PRIEST@soton.ac.uk*

[2]*School of Civil Engineering and the Environment, University of Southampton, Highfield,* SO17 1BJ, *UK*

Accepted 2005 October 7. Received 2005 September 23; in original form 2004 August 4

SUMMARY

Compressional wave (*P* wave) and shear wave (*S* wave) velocities (V_p and V_s, respectively) from remote seismic methods have been used to infer the distribution and volume of gas hydrate within marine sediments. Recent advances in seismic methods now allow compressional and shear wave attenuations (Q_p^{-1} and Q_s^{-1}, respectively) to be measured. However, the interpretation of these data is problematic due to our limited understanding of the effects of gas hydrate on physical properties. Therefore, a laboratory gas hydrate resonant column was developed to simulate pressure and temperature conditions suitable for methane gas hydrate formation in sand specimens and the subsequent measurement of both Q_p^{-1} and Q_s^{-1} at frequencies and strains relevant to marine seismic surveys. 13 dry (gas saturated) sand specimens were investigated with different amounts of methane gas hydrate evenly dispersed throughout each specimen. The results show that for these dry specimens both Q_p^{-1} and Q_s^{-1} are highly sensitive to hydrate saturation with unexpected peaks observed between 3 and 5 per cent hydrate saturation. It is thought that viscous squirt flow of absorbed water or free gas within the pore space is enhanced by hydrate cement at grain contacts and by the nanoporosity of the hydrate itself. These results show for the first time the dramatic effect methane gas hydrate can have on seismic wave attenuation in sand, and provide insight into wave propagation mechanisms. These results will aid the interpretation of elastic wave attenuation data obtained using marine seismic prospecting methods.

Key words: gas hydrates, laboratory resonant column, sand, seismic attenuation.

1 INTRODUCTION

Methane gas hydrates are crystalline compounds, which exist naturally in sediments on our continental margins, deep lakes and polar regions where permafrost is present. A volume of 1 m^3 of gas hydrates is able to store up to 164 times the equivalent volume of methane gas at STP (Sloan 1998). Potentially large volumes of methane gas can be released from hydrate-bearing sediments as a result of changes in temperature or pressure at the base of the hydrate stability zone (BHSZ). This can cause structural weakening of the sediment and may have been a possible mechanism for slope failures on continental margins in our geological past (Ashi 1999; Berndt *et al.* 2002; Kayen & Lee 1991; Mienert *et al.* 1998; Popenoe *et al.* 1993). Increasing drilling activity by oil exploration companies on deep water continental margins where hydrates form, and possible changes in ocean bottom water temperatures by global warming, have led to an increased focus on gas hydrates as a potential geological hazard.

High-resolution seismic methods provide a cost effective tool for detecting and delineating deposits in the upper 500 m beneath the seabed. They have been extensively used to identify and quantify gas hydrates in recent studies (Gettrust *et al.* 1999; Holbrook *et al.* 1996; Katzman *et al.* 1994; Korenaga *et al.* 1997; Minshull *et al.* 1994; Vanneste *et al.* 2002). Although the use of compressional wave velocity (V_p) is useful for delineating the change from a gas-free zone to a gas-bearing zone at the BHSZ, the quantification of the amount of gas hydrates above the gas zone has proven difficult to achieve because of uncertainties in the mechanical properties of the sediment as a result of the inclusion of gas hydrate. The use of more sophisticated seismic techniques has enabled other geophysical properties of the sediment to be measured including shear wave velocity (V_s), compressional wave attenuation (Q_p^{-1}) and shear wave attenuation (Q_s^{-1}) (Rossi *et al.* 2005). It is assumed that if the hydrate acts as a cementing agent then both Q_p^{-1} and Q_s^{-1} may be sensitive to small volumes of gas hydrate within the sediment (Pecher & Holbrook 2000). Wood *et al.* (2000) assumed that $Q_p^{-1}$and Q_s^{-1} would reduce for hydrate-bearing sediments in a similar manner to attenuation in frozen rocks (Toksöz *et al.* 1979), while Al-Hunaidi *et al.* (1996) showed that attenuation increases for clay soils when they are frozen. Therefore, when Wood *et al.* (2000) observed an increase in attenuation on vertical seismic profiles (VSPs) acquired on Ocean Drilling Program (ODP) Leg 164, it was attributed to the normal variance in attenuation for fine mud sediments. Guerin & Goldberg (2002) undertook a detailed analysis of sonic waveform

attenuation in hydrate-bearing sediments from well logs obtained from the Malik 2L-38 research well in the Mackenzie Delta, Canada. The results showed that both Q_p^{-1} and Q_s^{-1} increased with hydrate saturation with Q_s^{-1} being more sensitive to hydrate inclusion than Q_p^{-1}, although this apparent increase in attenuation was not evident in the amplitudes from seismic reflection data obtained from the same well (Collett *et al.* 1999). An apparent increase in Q_p^{-1} was previously identified from sonic well logs obtained on the Blake Ridge (Guerin *et al.* 1999). However, the poor quality of the borehole coupled with the low hydrate concentrations recorded prevented detailed conclusions to be drawn from the dataset. These results, therefore, provide conflicting views of the attenuative properties of hydrate-bearing sediments.

A more detailed understanding of the effect of gas hydrates on sediment physical properties, like seismic velocity and attenuation, is required to enable the use of seismic methods for evaluating the presence of gas hydrate *in situ*. In this paper the attenuative properties of laboratory prepared specimens of dry (gas saturated) sand containing differing volumes of methane gas hydrate within the pore space are presented. A specially constructed gas hydrate resonant column (GHRC) was used to measure both Q_E^{-1} (flexural-longitudinal wave attenuation) and Q_s^{-1} (torsional shear wave attenuation) of hydrate-bearing sand specimens at frequencies <400 Hz and at strains $<10^{-6}$ that are commonly employed in seismic surveys, and at pressures and temperatures suitable for hydrate stability (3.55 MPa, 4°C). The desired *P*-wave attenuation (Q_p^{-1}) was derived from its known relationship with Q_E^{-1}, Q_s^{-1} and Poisson's ratio (ν). A methodology was developed that ensured a homogeneous distribution of the hydrate throughout the specimen at predefined volumes of methane gas hydrate, thus allowing the observed changes in Q_p^{-1} and Q_s^{-1} to be related to known hydrate saturations. The results show an entirely unexpected peak in attenuation for all modes centred around 3–5 per cent hydrate saturation.

2 ATTENUATION MEASUREMENTS

The attenuation of seismic energy occurs primarily as the result of three differing phenomena;

(i) geometric spreading,
(ii) scattering, and
(iii) absorption of energy by the medium in which it is travelling.

Geometric spreading is independent of the material in which the elastic wave is travelling. Scattering tends to be significant only for wavelengths close to the size of any heterogeneities in the medium. Absorption, or intrinsic attenuation, is a function of the characteristics of the material (grain size, mineralogy, saturation, etc.) and the frequency of the elastic wave. The intrinsic attenuation, Q^{-1}, can be defined as the energy loss per cycle as the stress wave propagates through the material (O'Connell & Budanisky 1978),

$$\frac{1}{Q} = \frac{\phi}{4\pi W}, \tag{1}$$

where ϕ is a measure of the energy loss per cycle and W is the average energy stored per cycle. The term Q^{-1} is known as the specific dissipation function, and Q as the quality factor of the material.

2.1 Free vibration decay

In this paper the intrinsic attenuation of laboratory prepared specimens of hydrate-bearing sand were measured within the GHRC utilizing the free vibration decay method. Fig. 1 shows the set-up of the resonant column. A 140 mm high by 70 mm diameter

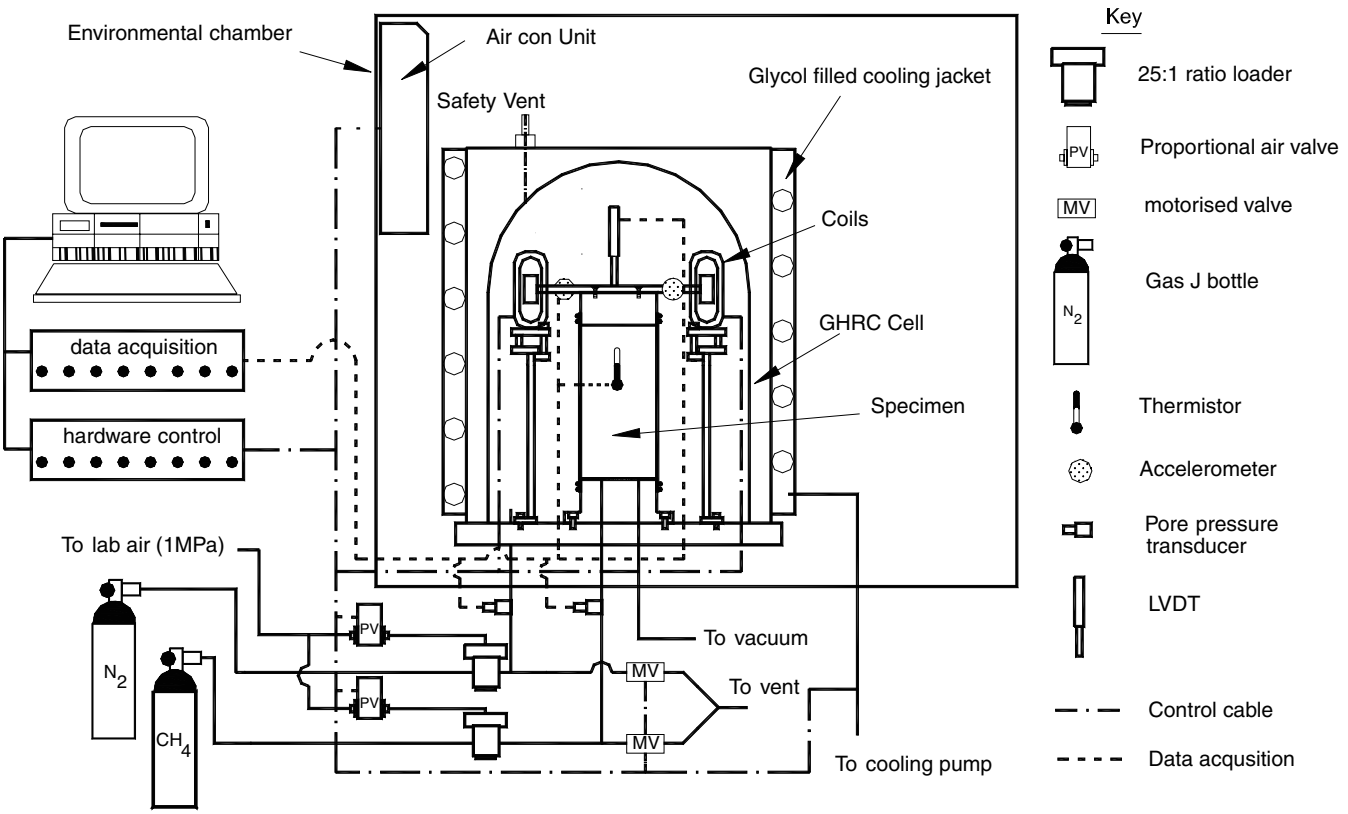

Figure 1. Schematic showing general layout of apparatus with pressure and temperature control, and data acquisition systems.

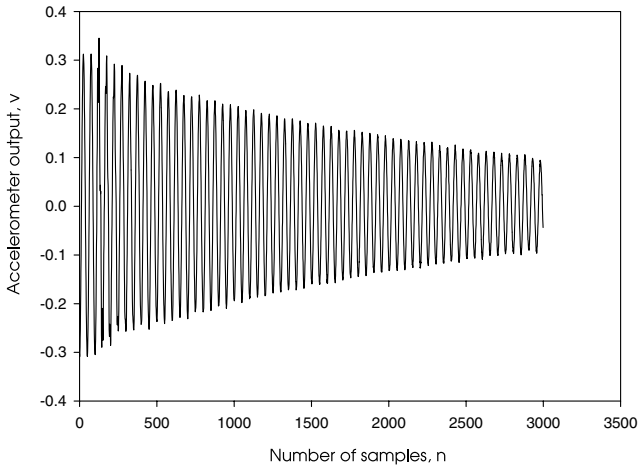

Figure 2. Typical free vibration decay response curve for a non-hydrate-bearing sand specimen.

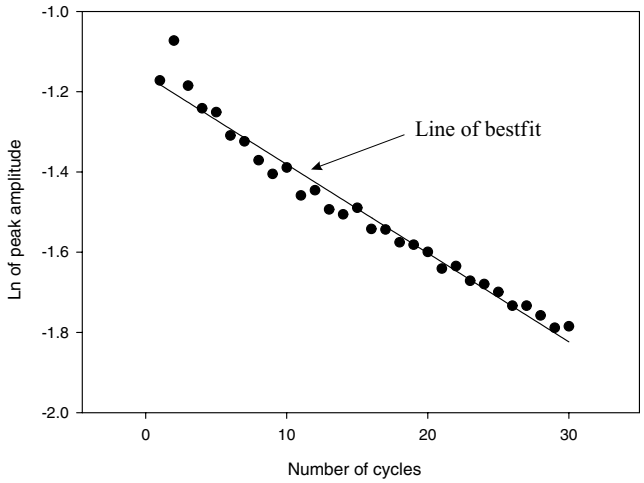

Figure 3. Plot of natural logarithm of peak amplitude against cycle number obtained from the free vibration decay curve in Fig 2. The logarithmic decrement, δ is obtained from the slope of the least-squares regression line fitted to the data.

specimen with the drive mechanism attached to its top is excited at its first mode of vibration. This is achieved by applying a sinusoidal voltage to a set of coils mounted on the support frame of the resonant column apparatus; the resultant magnetic field interacts with the permanent magnets attached to the drive mechanism causing the specimen and drive mechanism (system) to vibrate. Once the system is vibrating in a steady state at its first mode resonant frequency, the power to the coils is switched off, the response of the freely vibrating system is monitored, and the resulting decay curve for the specimen is digitally stored by the computer controlling the apparatus. Fig. 2 shows a typical free vibration decay response for a non-hydrate-bearing sand specimen. In a dissipative system the difference in amplitude between successive peaks can be interpreted as energy loss per cycle and is termed the logarithmic decrement δ. The logarithmic decrement can be expressed as

$$\delta = \ln \frac{A_1}{A_2}, \tag{2}$$

where A_1 and A_2 are the peak amplitudes of successive cycles. Fig. 3 shows the natural logarithm of peak amplitude for each cycle plotted against cycle number for the free vibration decay plot in Fig. 2. The logarithmic decrement can be found from the slope of the line of best fit through the data points in Fig. 3. The intrinsic attenuation (Q^{-1}) is related to the logarithmic decrement by the simple relationship

$$\frac{1}{Q} = \frac{\delta}{\pi}. \tag{3}$$

It is also worth noting that different attenuation modes are obtained for different measurement techniques. Therefore, dynamic methods such as the resonant column can measure shear wave attenuation Q_s^{-1} from torsional vibration, and longitudinal-flexural attenuation Q_E^{-1} (anelasticity of the Young's modulus, E Johnson & Toksöz 1981) from flexural excitation. The bulk modulus attenuation, Q_k^{-1} can be derived from hydrostatic stress and dilatational strain measurements, whereas seismic surveys provide compressional (P-) wave attenuation Q_p^{-1} that includes contributions from both Q_k^{-1} and Q_s^{-1}. For an isotropic medium these different attenuation values can be related to each other by the following expressions from Winkler & Nur (1979)

$$\begin{aligned} \frac{(1-\nu)(1-2\nu)}{Q_p} &= \frac{1+\nu}{Q_E} - \frac{2\nu(2-\nu)}{Q_s}, \\ \frac{(1-2\nu)}{Q_k} &= \frac{3}{Q_E} - \frac{2(\nu+1)}{Q_s}, \\ \frac{1+\nu}{Q_k} &= \frac{3(1-\nu)}{Q_p} - \frac{2(1-\nu)}{Q_s}, \end{aligned} \tag{4}$$

where ν is Poisson's ratio evaluated using

$$\nu = \frac{1}{2}\left(\frac{V_{lf}^2}{V_s^2}\right) - 1. \tag{5}$$

The parameters V_{lf} and V_s are the velocities obtained from resonant column tests using longitudinal-flexural and torsional vibration, respectively (Priest *et al.* 2005).

2.2 Apparatus calibration

In using the resonant column the measured attenuation is a combination of the intrinsic attenuation of the specimen and any inherent attenuation caused by the apparatus. The predominant error attributable to the apparatus is caused by the motion of the magnets through the coils. The applied voltage produces a magnetic field which interacts with the magnets and induces motion. However, once the power to the coils is shut off and the system is allowed to vibrate freely, the motion of the magnets through the coils induces a voltage in the coils, which opposes this motion. This is termed the back-EMF and the degree of attenuation attributable to it is frequency dependent (Meng & Rix 2003). Several differing methods have been adopted to reduce the influence of the equipment generated attenuation, which include using correction curves (Wang *et al.* 2003) or by using a current-mode source (Meng & Rix 2003). In this paper the attenuation caused by the back-EMF was negated by the design of a switching arrangement which allowed all the coils to be disconnected (i.e. open circuit) during free vibration decay. The provision of an open circuit prevents a back-EMF being induced in the coils and, therefore, eliminates its inertial effect on the vibrating system. Fig. 4 shows the measured attenuation using aluminium calibration bars in place of the specimen for both the open circuit

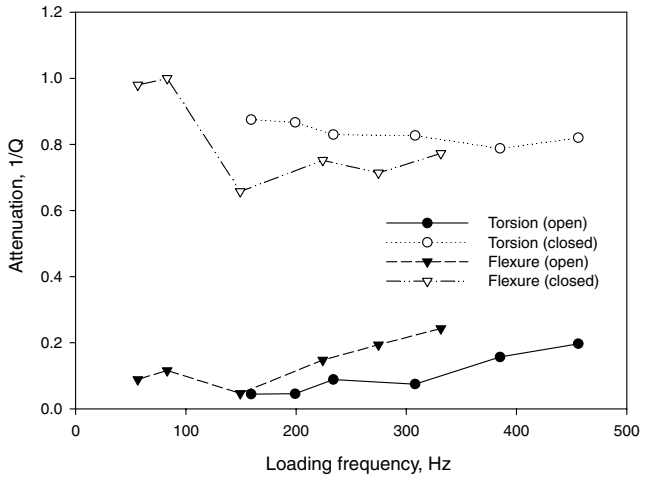

Figure 4. Measurement of attenuation using open-circuit (open) and closed circuit (closed) arrangements in torsional and flexural excitation for different aluminium calibration bars.

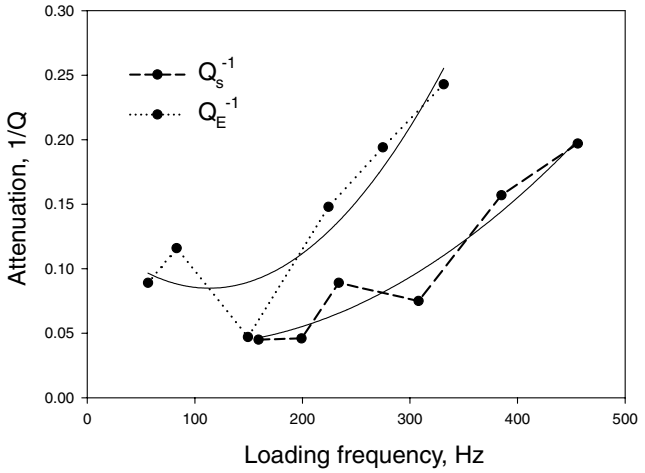

Figure 5. Flexural and torsional attenuation correction curves (lines of best fit) from regression analyses of the open-circuit attenuation data in Fig. 4.

and closed circuit arrangement. As the attenuation of the aluminium bars is negligible the increase in attenuation with frequency, which is observed for the open circuit arrangement is thought to possibly result from imperfect coupling of the various components of the drive mechanism. This error was removed from the attenuation results for the hydrate-bearing specimens by using correction curves for each mode of vibration, as shown in Fig. 5. It should also be noted that the attenuation is measured at the resonant frequency of the system and that the resonant frequency for the torsional mode does not necessarily correspond with the resonant frequency for the flexural mode.

3 SPECIMEN PREPARATION AND METHANE HYDRATE FORMATION

In total, 13 specimens of Leighton Buzzard sand with different volumes of methane gas hydrate within the pore space were tested within the resonant column. The initial properties of the specimen prior to hydrate formation are shown in Table 1. The sand was Leighton Buzzard Grade E, which is a uniform, rounded to subrounded, fine sand with 85 per cent by weight falling between

Table 1. Properties of test specimens.

Specimen no.	Added water as per cent of pore space	Initial porosity, $\sigma' = 250$ kPa	Porosity at $\sigma' = 500$ kPa with hydrate
HOL	0	0.465	0.463
H0D	0	0.416	0.413
H1	1.07	0.400	0.397
H2	2.16	0.419	0.412
H3-1	3.03	0.419	0.409
H3-2	2.72	0.443	0.431
H4-1	3.77	0.423	0.407
H4-2	3.85	0.430	0.429
H5-1	4.94	0.419	0.400
H5-2	4.91	0.423	0.424
H10	9.67	0.432	0.392
H20	18.06	0.428	0.353
H40	35.63	0.428	0.279

90 and 150 μm. Its minimum and maximum dry densities were found to be 1331 kg m^{-3} and 1624 kg m^{-3}, respectively (Cresswell *et al.* 1999; Kolbuszewski 1948; Rad & Tumay 1987; Walter *et al.* 1982). As a reference, two specimens were formed with no hydrate in the pore space but at differing densities, termed loose (H0L) and dense (H0D) (relative to the minimum and maximum dry densities for this sand). The formation of gas hydrate was achieved using a modified version of the technique developed by Stern *et al.* (1996), which formed hydrate from the slow melting of ice in the presence of methane gas at high pressure (>20 MPa). In our tests, a known mass of sieved, triply distilled, de-aired H_2O ice with a grain size between 180 and 250 μm was mixed with a known mass of dried frozen sand. Thorough mixing of the ice and sand with repeated use of a riffle box (an apparatus designed to produce two equal subsamples in the base trays when the constituents are emptied through a top grill) ensured a homogeneous distribution of ice within the sand. The ice was subsequently allowed to melt (in air-tight bags), and the liquid water was left to redistribute itself before this damp sand was used to form a specimen.

Specimens were made by tamping the moist sand in eight equal layers to form a sand specimen. The specimen was sealed within a butyl rubber membrane fixed to the base pedestal, and a top cap placed on the top of the sand. The use of a butyl membrane helped mitigate the migration of cell and pore pressure gases since standard latex membranes are known to be gas permeable (Bishop & Henkel 1962). Two thermistors were attached on each side of the specimen at mid-height to measure temperature change, and an LVDT was used to measure axial displacement.

The gas pressure and temperature regime followed during hydrate formation can be seen in Fig. 6. Once the specimen was formed and the external dimensions of the specimen taken, the drive mechanism and pressure cell were secured in place. An effective stress of 250 kPa [at point (a) in Fig. 6] was applied to the specimen under atmospheric back pressure. The specimen temperature was then reduced to -15°C causing the interstitial pore water to freeze [point (b) in Fig. 6]. Once the specimen temperature was stabilized, the nitrogen cell and methane back pressure were slowly raised to a back pressure of 15 MPa over about 1.5 hr while maintaining an effective confining pressure of 250 $\pm$ 50 kPa on the specimen [point (c) in Fig. 6]. The formation of gas hydrate was then initiated by slowly raising the temperature of the specimen from -15°C to 10°C [points (c) to (d) in Fig. 6], where it was held for a further 10–15 hours. The high back pressure applied to the specimen was used to enable a quick conversion of ice to hydrate (Hwang *et al.* 1990). Once full hydrate conversion was deemed to have occurred the back pressure

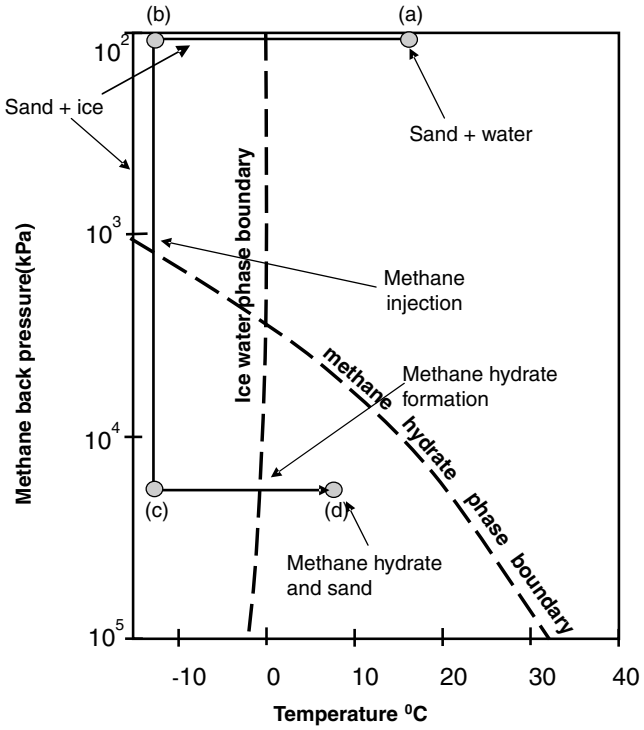

Figure 6. The methane hydrate formation procedure showing variations in the pressure and temperature regime.

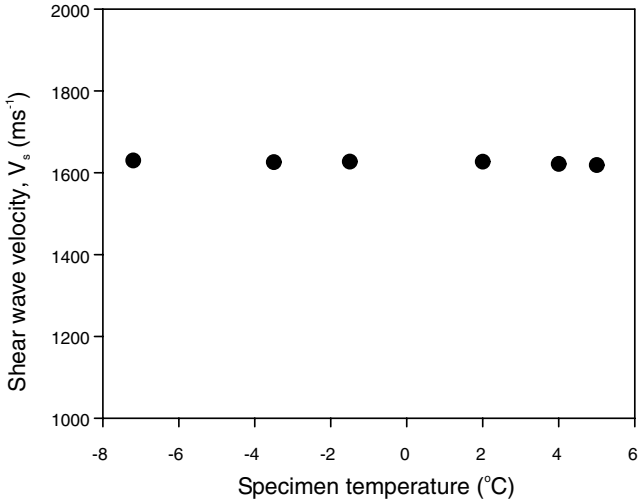

Figure 7. Variation in shear wave velocity, V_s with temperature, °C for a sand specimen with a hydrate content of 36 per cent.

was reduced to 5 MPa (with the same 250 kPa effective confining pressure being maintained) and the specimen temperature to 3°C, ready to commence the resonant column testing.

3.1 Testing procedure

The measurement program was designed to characterize the attenuative properties of dry (gas saturated) sand specimens containing differing volumes of methane gas hydrate within the pore space under isotropic loading and unloading. Isotropic loading was applied in steps of 250 kPa up to an effective stress (σ') of 2000 kPa, with the unloading steps following the same sequence in reverse. Attenuation measurements were obtained at each loading and unloading step. Each load step was maintained for thirty minutes to allow initial consolidation of the specimen to occur before resonant testing was undertaken.

Tests on dry Leighton Buzzard sand had shown that for strains below 10^{-5}, attenuation is nearly independent of strain amplitude (Priest 2004). This transition from the 'elastic' response to the strain dependent response is termed the elastic threshold γ_t^e. Above this value, the non-linear losses are attributable to intergranular friction (Winkler *et al.* 1979). Therefore, measurements of attenuation obtained in the resonant column when the applied strain is kept below γ_t^e can be considered to be representative of small strain measurements obtained during seismic surveys. As the applied strain is a function of the peak amplitude measured by the accelerometer at resonance, the applied strain can be easily quantified for each test run. All measurements presented here were recorded at strains below γ_t^e (10^{-6}).

3.2 Estimation of hydrate volume

It was assumed that hydrate formation would occur once the specimen temperature had risen above 0°C and that the hydrate volume could be estimated by measuring the volume of methane consumed during the formation process (Stern *et al.* 1996). However, due to hydrate formation commencing during the rise in methane pore pressure up to 15 MPa and continuing while the specimen temperature was raised to 0°C, this technique was unfeasible. Therefore, as hydrate forms from gas and water the volume of hydrate within each specimen was assumed to be proportional to the volume of ice added to the sand. The inherent moisture of the sand prior to mixing with the ice was measured and shown to be on average 2.36 g/1000 g of sand. This inherent moisture was not included in the calculations of the volume of hydrate within the pore space.

To validate the assumption that all the added water was converted to hydrate, tests were conducted to determine the shear wave velocity for a specimen containing an assumed hydrate saturation of 36 per cent, as the temperature was lowered from 5°C to −7.2°C. Fig. 7 shows the shear wave velocity as a function of specimen temperature. It can be seen that a maximum increase of 0.6 per cent in shear velocity was observed as the temperature was lowered to −7.2°C, suggesting that there was some free water left in the specimen, although causing a negligible change in velocity compared to the effect of different target hydrate contents (see below).

4 RESULTS AND DISCUSSION

4.1 Intrinsic attenuation in hydrate-bearing sand

Fig. 8 shows the variation of shear wave attenuation, Q_s^{-1} and longitudinal wave attenuation, Q_E^{-1} for a variety of gas saturated hydrate-bearing sand specimens. The inclusion of hydrate into the pore space causes an increase in attenuation for both modes of vibration. The attenuation values as a function of σ' (Fig. 8) show a high degree of scatter for each specimen, although the general trend exhibits a low sensitivity to σ'. Fig. 9 shows attenuation Q_s^{-1} and Q_E^{-1}, for selected specimens (H0D, H3-2 and H40) with error bars showing the 95 per cent confidence limits for the measured data. The values for the error bars were obtained by applying a 95 per cent confidence limit to the least-squares regression curve fitted through the measured values of peak amplitude per cycle for each free vibration decay test (Fig. 3). Although the error bars are large for certain measurements, the results show that the increase in attenuation due to the inclusion of

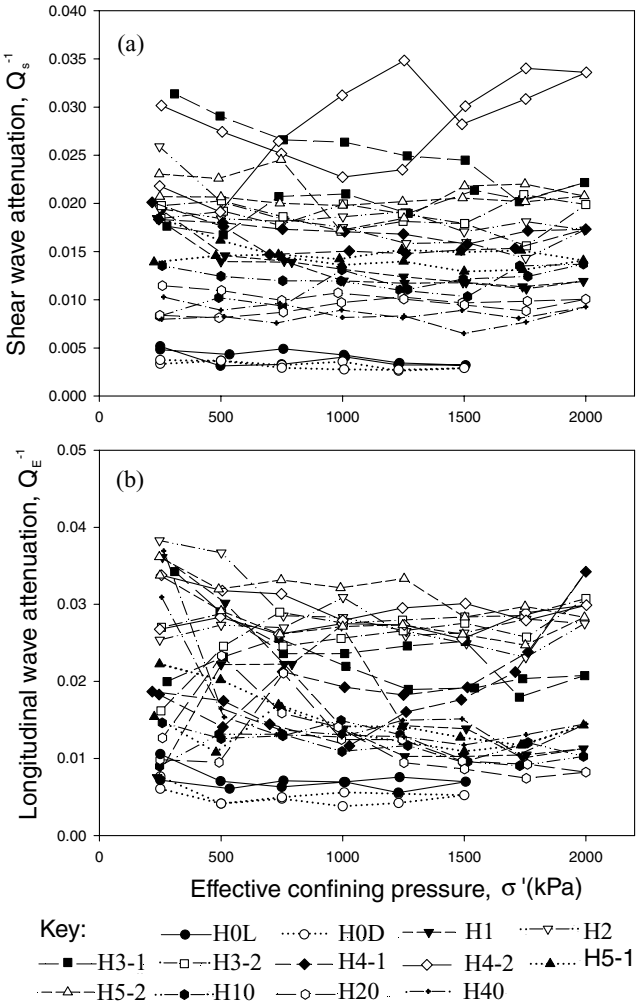

Figure 8. (a) Shear wave attenuation Q_s^{-1} and (b) longitudinal wave attenuation Q_E^{-1} as a function of effective confining pressure (σ') for all specimens listed in Table 1.

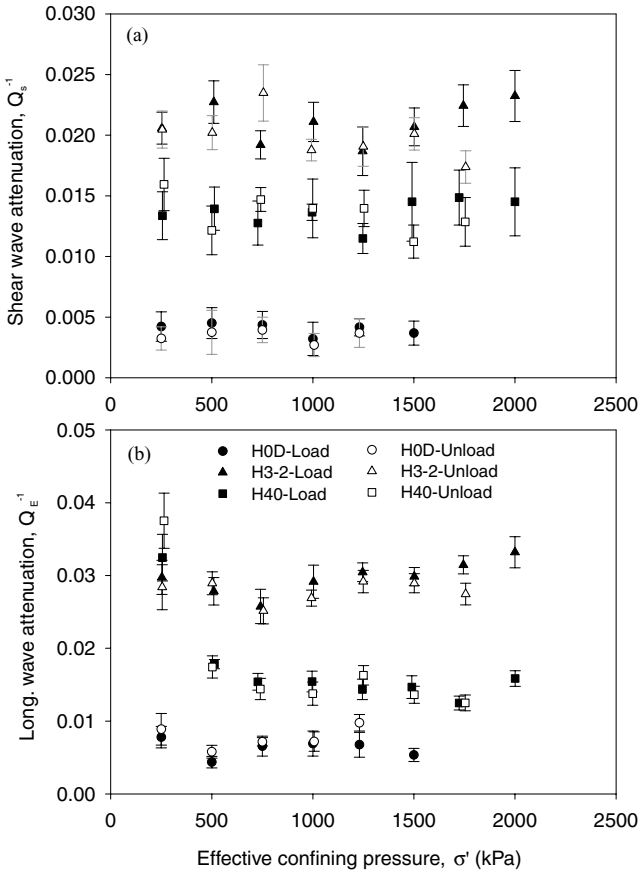

Figure 9. (a) Shear wave, Q_s^{-1} and (b) longitudinal wave attenuation, Q_E^{-1} against effective confining pressure, σ' for specimens H0D, H3-2 and H40 with error bars.

hydrate is significantly larger than the errors arising from the measurement technique. A comparison of attenuation between Figs 8(a) and (b) shows that the longitudinal wave attenuation is more variable than shear wave attenuation, and shows an increased sensitivity to changes in effective confining pressure within each specimen. A comparison of Q_s^{-1} and Q_E^{-1} with hydrate saturation at an effective confining pressure of 500 kPa is shown in Fig. 10. The trend lines for the attenuation values show that small amounts of hydrate have a major influence on attenuation with a clearly defined peak observed around 3–5 per cent hydrate saturation. This attenuation peak corresponds to a transition zone, that was observed in the seismic velocity measurements (compressional velocity, V_p and shear wave velocity V_s) obtained from the same hydrate-bearing specimens (Priest *et al.* 2005). These values are shown in Fig. 11; as the specimens were saturated with gas, water saturated velocities were calculated using Gassmann's (1951) equation, which is explained in detail in Priest *et al.* (2005). The transition zone is identified by the change in the slope of the velocity curve with hydrate saturation at 3–5 per cent hydrate saturation. It is suggested that this zone corresponds to cementation by the hydrate of the sand grain contacts throughout the specimen (Priest *et al.* 2005) . After the attenuation peak at 3–5 per cent hydrate saturation in Fig. 10, attenuation reduces to a value still generally two to three times higher than that for specimens with no hydrate (H0L and H0D), which then increases gradually with hydrate saturation up to the maximum hydrate saturation around 36 per cent. Similar attenuation peaks were reported by Saxena *et al.* (1988) for sand specimens cemented by ordinary Portland cement where the attenuation peak corresponded to a 5–8 per cent cement saturation (by mass of the specimen) and decreased thereafter.

The relationship between the calculated *P*-wave attenuation, Q_p^{-1}, bulk attenuation, Q_k^{-1} and hydrate saturation are shown in Fig 12. Error bars are shown, which highlight the range of possible values due to systematic errors and uncertainties in the determination of V_{lf} (Priest 2004) when used in eq. 5. The added trend lines show that Q_p^{-1} and Q_k^{-1} follows the same trend identified for $Q_s^{-1}$and Q_E^{-1} as highlighted in Fig. 10. However, it can be seen that the values of Q_p^{-1} and Q_k^{-1} obtained for specimens H4-1 and H5-1 lie considerably outside these trend lines.

The values of Q_p^{-1} and Q_k^{-1} are dependent on the value of Poisson's ratio, computed from eq. (5), the velocities derived from the resonance frequencies of the specimen (Priest *et al.* 2005), and the measured values of Q_s^{-1} and Q_E^{-1} at each load step. Fig. 13 shows the computed Poisson's ratio for each specimen as a function of hydrate saturation at an effective confining pressure of 500 kPa. Again, error bars are provided to show the range of possible values due to systematic errors and the uncertainty with V_{lf} (longitudinal-flexural velocity measured in the resonant column). The measured values for Poisson's ratio for the non-hydrate-bearing specimens is commensurate with that for unconsolidated sands (Cascante *et al.*

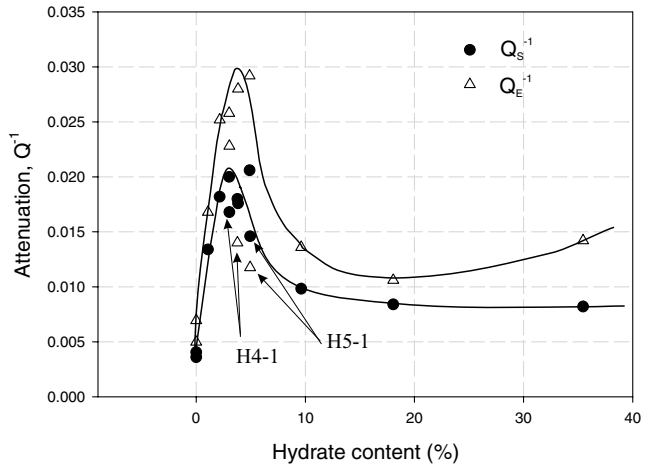

Figure 10. Shear wave attenuation Q_s^{-1}, and longitudinal wave attenuation Q_E^{-1} as a function of hydrate saturation for all specimens at an effective confining pressure of 500 kPa. Lines are drawn to show general trends.

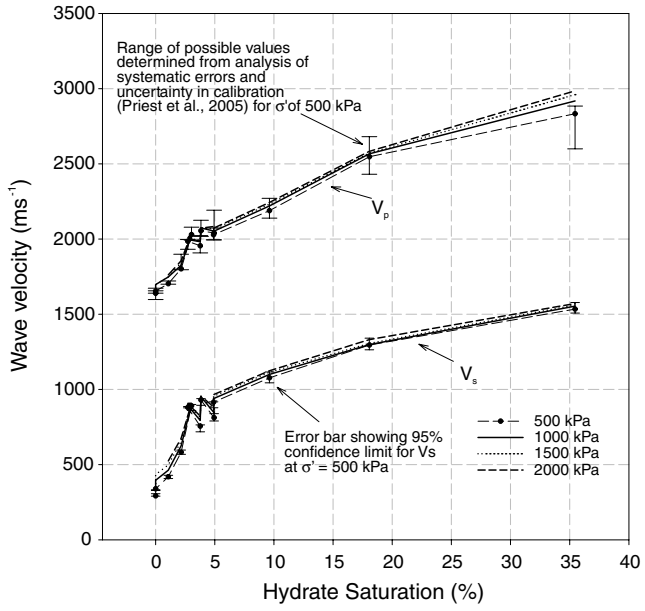

Figure 11. Variation in water saturated V_p and V_s with hydrate pore saturation for specimens listed in Table 1 at a range of effective stresses, σ after Priest *et al.* (2005). Error bars show the uncertainty in values due to systematic and calibration errors at $\sigma' = 500$ kPa. Velocities were calculated using Gassmann's equation.

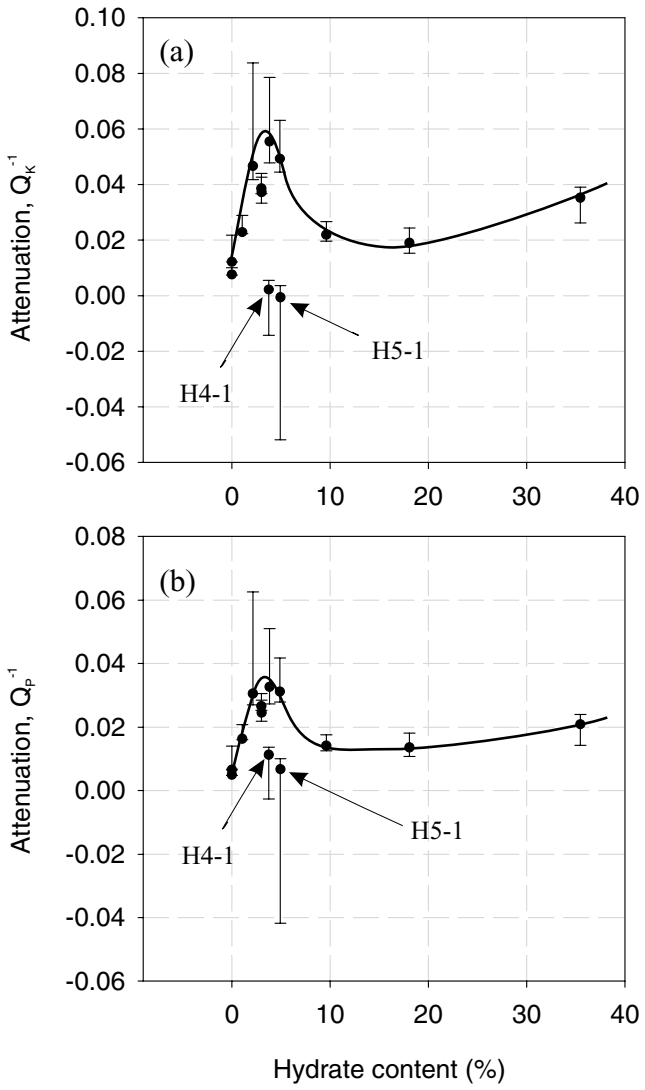

Figure 12. (a) Bulk compressional attenuation, Q_k^{-1} and (b) compressional wave attenuation, Q_p^{-1} as a function of hydrate saturation at $\sigma' = 500$ kPa for all specimens.

1998), given the possible errors. As the hydrate saturation increases, the Poisson's ratio increases to around 0.2, which is close to that found for dry sandstones (Han *et al.* 1986; Strandenes & Blangy 1991). The results show the Poisson's ratio computed for H5-1 to be much higher than that for the other specimens with low hydrate saturation, with specimen H4-1 being only slightly higher. The high values of Poisson's ratio, coupled with the low attenuation values of Q_E^{-1} observed for both specimens, results in the very low attenuation values for both Q_p^{-1} and Q_k^{-1} seen in Fig. 12.

It is also noted that the largest errors in both Q_p^{-1} and Q_k^{-1} occur at the peak in attenuation for specimens with hydrate saturation between 3 and 5 per cent, which corresponds to the attenuation peak noted for Q_s^{-1}. It has been shown by Priest *et al.* (2005) that all the sand grains in the specimen become fully cemented by the hydrate over this range of hydrate saturation, which leads to variability in *P*- and *S*-wave velocity (patchy cementation occurs below 3–5 per cent). This suggests that both attenuation and velocity measurements are sensitive to the distribution and bonding of hydrates in the sand over this range of critical hydrate saturation.

It is generally assumed that the presence of gas hydrates in the pore space of marine sediments causes a reduction in attenuation (Guerin & Goldberg 2002; Pecher & Holbrook 2000) due to a reduction in porosity, based on experimental results by Hamilton (1972). This hypothesis is dependent on frictional losses at grain contacts being the main source of attenuation. However, testing of Leighton Buzzard sand shows that attenuation is constant for strains smaller than the linear threshold value of 10^{-5} and outside the influence of intergranular friction (Winkler & Nur 1979). All measurements of attenuation undertaken as part of this research were performed at strains $<10^{-6}$, which precludes intergranular friction as a dominating loss mechanism.

Therefore, we have developed a qualitative, conceptual model to describe the observed attenuation in hydrate-bearing sediments saturated with methane gas based on the assumption that losses

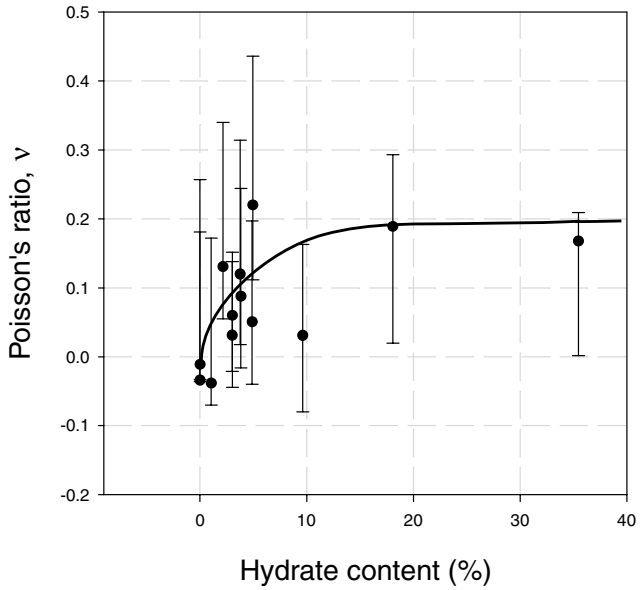

Figure 13. Poisson's ratio (ν) derived from V_s and V_{lf} measurements for all specimens as a function of hydrate saturation at $\sigma' = 500$ kPa. Error bars show the range of values due to uncertainties in the measurement of V_{lf} (Priest *et al.* 2005).

result from viscous fluid flow (either absorbed water or free gas) in cracks or small pores of low aspect ratio, as suggested by Mavko & Nur (1979). Literature on frozen porous media has shown that the surfaces of soil particles remain liquid water wet in the presence of water ice (Handa *et al.* 1992; Overloop & Van Gerven 1993; Tsytovich 1975; Valiullin & Furo 2002). As many physical characteristics of ice and hydrate are similar, it can be surmised that after hydrate formation small volumes of liquid water remain as adsorbed water on the sand grains.

Fig. 14 idealizes the differing stages of hydrate formation and their possible effect on attenuation in sands due to the formation of hydrate cement at grain contacts. Although a pore filling model is generally preferred to a cement contact model, recent research has suggested that in certain environments hydrate acts as a load-bearing cement (Chand & Minshull 2004; Chand *et al.* 2004; Stern *et al.* 2005). For the air dry sand specimens (Fig. 14a) a small volume of adsorbed water (all specimens contained approx. 2 g of adsorbed water) is contained within the pore space of the sands. Due to surface tension and capillary pressures this water will preferentially, but not exclusively, condense at sand grain contacts. During the passing of a seismic wave these grain contacts are deformed momentarily causing dissipative fluid flow of adsorbed water (and or free gas) back and forth from this deformed zone. Attenuation is minimal because of the small volume of adsorbed water, which may not fill many grain contact micropores, and the total area of the grain contact is relatively small (Fig. 14a). As the density of the sand increases from the loose sand specimen H0L to the dense sand specimen H0D (see Table 1), the stability of grain contacts increases resulting in a reduction in the transient deformation magnitudes of grain contacts. This effect seems to dominate over the effect of the more numerous grain contacts in the dense specimen (and hence more sites for squirt flow), resulting in a reduction in the observed attenuation between the loose and dense dry sand specimens.

Fig. 14(b) idealizes hydrate growth in the pore space at grain boundaries causing cementation of grain contacts, which in turn leads to an increase in effective area of the grain contact. By assuming that the cementation of the sand grains by hydrate is not perfect across the whole region, similar to cemented sandstones (Murphy *et al.* 1986), the idealized crack length at the grain contact area is increased (due to increased cementation). Therefore, as the hydrate saturation increases up to the critical hydrate saturation value of

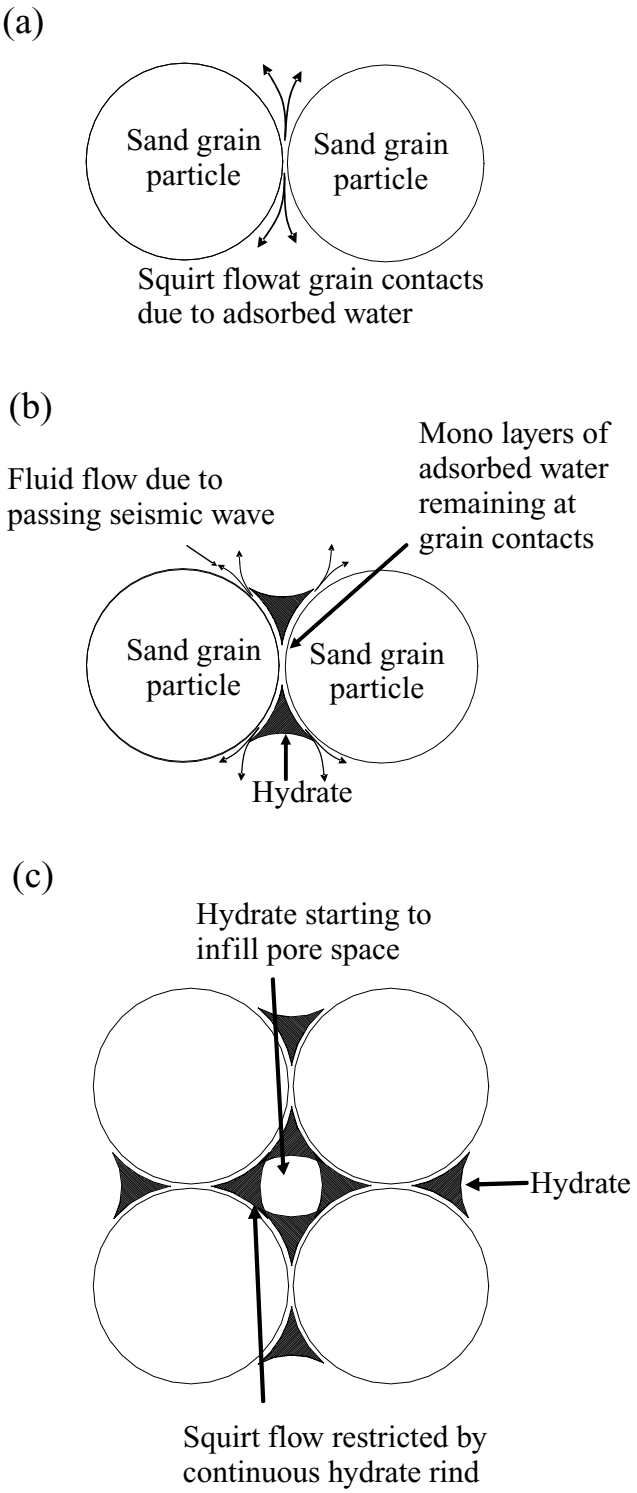

Figure 14. Conceptual model of cemented grain contacts with increasing hydrate saturation. (a) Idealized view of sand grain contact with no hydrate. (b) Grain contacts with hydrate growing at grain boundaries. (c) Connected hydrate cementing grain contacts with commencement of pore filling.

3–5 per cent the number of cemented grain contacts increase with a corresponding increase in attenuation.

At some point over the critical range of hydrate saturation all sand grains become cemented and attenuation reaches a maximum. Above the critical hydrate saturation range, increasing hydrate leads to an encasement of the sand grains and an infilling of the pore space (Fig. 14c). As the sand grains become encased the potential for squirt flow into the equant pore space is reduced, or impeded, which in turn leads to a reduction in attenuation. The attenuation measured on specimens containing higher hydrate concentrations are twice those measured on air dry specimens, suggesting that only partial impediment of the squirt-flow phenomena occurs. It has been shown that hydrate (both laboratory and natural) has a porous structure (Salamatin & Kuhs 2002; Staykova *et al.* 2002, 2003; Stern *et al.* 2005) with pore sizes for methane gas hydrate ranging from 100 to 400 nm. This may, therefore, suggest that as the hydrate seals around the sand grains and reduces the fluid flow through the flat cracks, there may still be some contribution to attenuation from fluid flow through the pores of the porous hydrate structure itself (Chand & Minshull 2004). Alternatively there may be fewer crack-like pores of the correct size to facilitate squirt flow at these frequencies (some authors suggest that squirt flow is related to signal frequency as well as pore size, geometry and pore fluid viscosity, e.g. Murphy *et al.* (1986).

Attenuation data from the Malik 2L-38 well in the Mackenzie Delta, Canada (Guerin & Goldberg 2002) showed a monotonic increase in attenuation up to 80 per cent hydrate saturation with Q_s^{-1} being higher than Q_P^{-1}, which is somewhat different from what was observed in these laboratory experiments. However, it has to be remembered that our tests were conducted on partially saturated specimens where the sediments at the Malik 2L–38 well were fully saturated. In partially saturated rocks $Q_P^{-1}$is greater than Q_s^{-1} due to the large compressibility of the gas which is not evident when rocks are fully saturated (Mavko & Nur 1979; Murphy 1982). Secondly, although the results of this research show limited evidence for increasing attenuation with hydrate saturation after the initial maximum (all results except for Q_s^{-1} show small increases in attenuation with hydrate saturation after the initial attenuation peak), this could be explained by the very small amount of free water available in each test since low saturation levels would lead to lower attenuation values than when fully saturated (Murphy 1982). Hence, seismic models are required that can use the current level of information to predict seismic attenuation in saturated, hydrate-bearing sand. This topic will be addressed in a later paper.

4.2 Attenuation in dissociated specimens

After testing, the hydrate-bearing specimens were allowed to dissociate in a controlled manner ensuring a constant effective confining pressure of 250 kPa was maintained at all times. Once fully dissociated, the specimens were tested under similar pressure conditions to when they contained hydrate. Fig. 15 shows the attenuation values for Q_s^{-1} and Q_E^{-1} from selected dissociated specimens, along with hydrate-bearing specimen H3-2 for comparison. It can be seen for the dissociated specimens that the measured attenuation has become pressure dependent, which is not seen in the attenuation values measured for the dry specimens or the hydrate-bearing specimens in Fig. 7. This pressure dependency may result from the closure of saturated micro-cracks at grain contacts (Best 1997) given that these specimens contain moisture, higher than the amount of adsorbed water in specimens H0L and H0D. Fig. 15 also shows that attenuation does not significantly increase as the volume of water, taken as a percentage of the pore space (i.e. saturation level), increases from 2 to 36 per cent, with no defined peak for specimens with hydrate (water) saturations between 3 and 5 per cent.

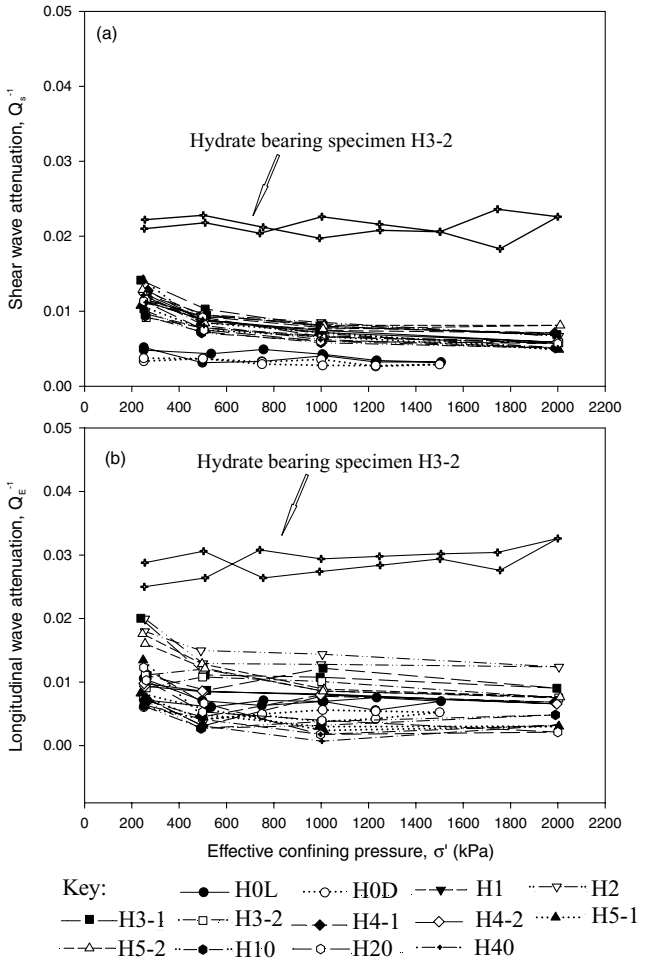

Figure 15. (a) Shear wave attenuation Q_s^{-1} and (b) longitudinal wave attenuation Q_E^{-1} as a function of effective confining pressure (σ') for selected specimens after hydrate dissociation. Hydrate-bearing specimen H3-2 shown for comparison.

5 CONCLUSIONS

Elastic wave attenuation measurements from marine seismic surveys can be used to estimate the distribution and volume of methane hydrate within ocean sediments based on the laboratory resonant column results reported in this study. For the first time, the variation in compressional and shear wave attenuations (Q_p^{-1} and Q_s^{-1}, respectively) in laboratory prepared specimens of methane gas hydrate-bearing sand, which were gas saturated, have been measured at seismic frequencies and strains as a function of hydrate saturation. The formation procedure forced hydrate growth to occur at grain contacts causing cementation of the sand grains, which may occur in nature in gas rich environments.

A laboratory apparatus (the gas hydrate resonant column or GHRC) was developed to allow measurement of the free vibration decay of a resonating specimen, from which its elastic wave attenuation properties can be calculated. Specific design improvements were implemented to allow the intrinsic attenuation attributable to

the apparatus to be removed, which greatly improved the accuracy of the attenuation measurements obtained. The resonant column was also modified to excite the specimen in the fundamental mode of longitudinal flexure as well as in torsion, thus enabling both compressional and shear wave attenuations (Q_p^{-1} and Q_s^{-1}) to be derived at frequencies less than 400 Hz and at strain levels less than 10^{-6}.

The attenuation of seismic waves within hydrate-bearing sands was shown to be sensitive to the volume of gas hydrate within the pore space. An attenuation peak was observed when the percentage of hydrate within the pore space was between 3 and 5 per cent. The measured attenuation was insensitive to effective confining pressure in the hydrate-bearing sand. A conceptual model was proposed to explain the observations. The peak in attenuation is thought to be due to cementation of grain contacts leading to an increase in low aspect ratio cracks between the hydrate and sand grains. This increase in the effective area of the grain contacts led to increased dissipation of mechanical wave energy due to the flow of adsorbed water (and or free gas) along the crack into the open pore space, and then back again during the passage of a seismic wave. Full encasement of the grains at higher hydrate saturation reduced the potential for fluid flow into the pore space, although fluid flow was still possible through the nanoporous hydrate, which may have higher aspect ratio pores than at grain contacts.

Attenuation measurements on dissociated specimens do not show any appreciable attenuation peak and only a small increase in attenuation from the air dry specimens due to the increase in water at grain contacts. Once the grain contacts were saturated, no appreciable change was noted with increasing water saturation. Also, the dissociated specimens showed sensitivity to the effective confining pressure, which was not observed in the same specimens when they contained hydrate.

List of Symbols

δ	logarithmic decrement.
γ_e^t	elastic strain threshold.
σ'	effective confining pressure, kPa.
ϕ	energy loss per cycle.
ν	Poisson's ratio.
A_1, A_2	amplitude of successive cycles during free vibration decay.
Q_E^{-1}	longitudinal wave attenuation.
Q_k^{-1}	bulk compressional attenuation.
Q_p^{-1}	compressional wave attenuation.
Q_s^{-1}	shear wave attenuation.
V_{lf}	longitudinal-flexural wave velocity, ms^{-1}.
V_p	compressional wave velocity, ms^{-1}.
V_s	shear wave velocity, ms^{-1}.
W	average energy stored per cycle.

ACKNOWLEDGMENTS

This work was funded under contract EVK3-CT-2000-00043 (HYDRATECH) of the European Commission and by the United Kingdom Natural Environment Research Council. JAP also received support from UK EPSRC PhD studentship no. 00310758. The resonant column was designed and built in collaboration with GDS Limited, UK with advice from C. McCann and J. Sothcott.

REFERENCES

Al-Hunaidi, M.O., Chen, P.A., Rainer, J.H. & Tremblay, M., 1996. Shear moduli and damping in frozen and unfrozen clay by resonant column tests, *Canadian Geotechnical Journal,* **35,** 510–514.

Ashi, J., 1999. Large submarine landslides associated with decomposition of gas hydrates, *Landslide News,* **12,** 17–19.

Berndt, C., Mienert, J., Vanneste, M., Bunz, S. & Bryn, P., 2002. Submarine slope-failure offshore Norway triggers rapid gas hydrate decomposition, *Proc. Fourth Int. Conf. On Gas Hydrates*, Yokohama, Japan, 71–74.

Best, A.I., 1997. The effect of pressure on ultrasonic velocity and attenuation in near-surface sedimentary rocks, *Geophs. Prospect.,* **45**(2), 345–364.

Bishop, A.W. & Henkel, D.J., 1962. *The Measurement of Soil Properties in the Triaxial Test*, Edward Arnold, London.

Cascante, G., Santamarina, C. & Yassir, N., 1998. Flexural excitation in a standard torsional-resonant column, *Can. Geotech. J.,* **35,** 478–490.

Chand, S. & Minshull, T.A., 2004. The effect of hydrate content on seismic attenuation: a case study for Malik 2L-38 well data, Mackenzie delta, Canada, *Geophys. Res. Lett.,* **31,** L14609, doi:14610.11029/12004GL020292.

Chand, S., Minshull, T.A., Gei, D. & Carcione, J.M., 2004. Elastic velocity models for gas-hydrate bearing sediments—a comparison, *Geophys. J. Int.,* **159**(2), 573–590.

Collett, T.S., Lee, M.W., Dalimore, S.R. & W.F. Agena, 1999. Seismic and well-log-inferred gas hydrate accumulations on Richards Island, in *Scientific Results from JAPEX/JNOC/GSC Malik 2L-38 Gas Hydrate Research Well, Mackenzie Delta, Northwest Territories, Canada*, pp. 357–376, eds Dallimore, S.R., Uchida, T. & Collett, T.S., Bull. Geol. Surv. Can., 544.

Cresswell, A., Barton, M.E. & Brown, M.R., 1999. Determining the maximum dry density of sands by pluviation, *Geotechnical Testing Journal,* **22**(4), 324–328.

Gassmann, F., 1951. Ueber die Elastizitaet poroeser Medien, *Vieteljahrsschrift der Naturforschenden Gessellschaft in Zuerich,* **96,** 1–23.

Gettrust, J., Wood, W. & Lindwall, D., 1999. New seismic study of deep sea hydrates results in greatly improved resolution, *EOS, Trans. Am. geophys. Un.,* **80,** 439–442.

Guerin, G. & Goldberg, D., 2002. Sonic waveform attenuation in gas hydrate-bearing sediments from the Malik 2L-38 research well, Mackenzie Delta, Canada, *J. geophs. Res.,* **107**(B5), EPM 1–EPM 11.

Guerin, G., Goldberg, D. & Meltser, A., 1999. Characterization of in situ elastic properties of gas hydrate-bearing sediments on the Blake Ridge, *J. geophys. Res.,* **104,** 17 781–17 795.

Hamilton, E.L., 1972. Compressional-wave attenuation in marine sediments, *Geophysics,* **37,** 620–646.

Han, D., Nur, A. & Morgan, D., 1986. Effects of porosity and clay content on wave velocities in sandstone, *Geophysics,* **51,** 2093–2107.

Handa, Y.P., Zakrzewski, M. & Fairbridge, C., 1992. Effect of restricted geometries on the surface and thermodynamic properties of ice, *J. Phys. Chem.,* **96,** 8594–8599.

Holbrook, W.S., Hoskins, H., Wood, W.T., Stephen, R.A., Lizzarralde, D. & the Leg 164 Science Party, 1996. Methane gas-hydrate and free gas on the Blake Ridge from vertical seismic profiling, *Science,* **273,** 1840–1843.

Hwang, M.J., Wright, D.A., Kapur, A. & Holder, G.D., 1990. An experimental study of crystallization and crystal growth of methane hydrates from melting ice, *J. Inclusion Phenom.,* **8,** 103–116.

Johnson, D.H. & Toksöz, M.N., 1981. Definitions and Terminology, in *Seismic wave attenuation, Geophysics reprint series*, Vol. 2, pp. 1–5, eds Toksoz, M.N. & Johnson, D.H., Society of Exploration Geophysics, Washington, DC.

Katzman, R., Holbrook, W.S. & Paull, C.K., 1994. Combined vertical incidence and wide-angle seismic study of a gas hydrate zone, Blake Ridge, *J. geophys. Res.,* **99**(B9), 17 975–17 995.

Kayen, R.E. & Lee, H.J., 1991. Pleistocene slope instability of gas hydrate-laden sediment on the Beaufort Sea margin, *Marine Geotechnology,* **10,** 125–141.

Kolbuszewski, J.J., 1948. An experimental study of the maximum and minimum porosities of sands, *Proceedings of the Second International Conference of Soil Mechanics and Foundation Engineering*, Rotterdam, **1,** 158–165.

Korenaga, J., Holbrook, W.S., Singh, S.C. & Minshull, T.A., 1997. Natural gas hydrates on the southeast US margin: constraints from full waveform and travel time inversions of wide-angle seismic data, *J. geophys. Res.,* **102**(B7), 15 345–15 365.

Mavko, G. & Nur, A., 1979. Wave attenuation in partially saturated rocks, *Geophysics,* **44,** 161–178.

Meng, J. & Rix, G.J., 2003. Reduction of equipment-generated damping in resonant column measurements, *Geotechnique,* **53**(5), 503–512.

Mienert, J., Posewang, J. & Baumann, M., 1998. Gas hydrates along the northeastern Atlantic margin: possible hydrate-bound margin instabilities and possible release of methane, in *Gas Hydrates: Relevance to World Margin Stability and Climate Change*, Vol. 137, pp. 275–291, eds Henriet, J.-P. & Mienert, J., Geological Society, Special Publications, London.

Minshull, T., Singh, S. & Westbrook, G., 1994. Seismic velocity structure of a gas hydrate reflector, offshore Western Columbia, from full waveform inversion, *J. geophys. Res.,* **99,** 4715–4734.

Murphy, W.F., 1982. Effects of partial saturation on attenuation in Massilon sandstone and Vycor porous glass, *J. acoust. Soc. America,* **71**(6), 1458–1468.

Murphy, W.F., Winkler, K.W. & Kleinberg, R.L., 1986. Acoustic relaxation in sedimentary rocks: Dependence on grain contacts and fluid saturation, *Geophysics,* **5,** 757–766.

O'Connell, R.J. & Budanisky, B., 1978. Measure of dissipation in viscoelastic media, *Geophys. Res. Lett.,* **5,** 5–8.

Overloop, K. & Van Gerven, L., 1993. Freezing phenomena in adsorbed water as studied by NMR, *J. Magn. Reson., Ser. A,* **101,** 179–187.

Pecher, I.A. & Holbrook, W.S., 2000. Seismic methods for detecting and quantifying marine methane hydrate/free gas reservoirs, in *Natural Gas Hydrates in Oceanic and Permafrost Environments*, pp. 275–294, ed. Max, M.D., Kluwer Academic Press, Norwell, Massachusetts.

Popenoe, P., Schmuck, E. & Dillon, W., 1993. The Cape Fear landslide: Slope failure associated with salt diapirism and gas hydrate decomposition, in *Submarine Landslides: Selective studies in the US Exclusive Economic Zone*, pp. 40–53, ed. Schwab, W., US Geological Survey Bulletin 2002.

Priest, J.A., 2004. The effects of methane gas hydrate on the dynamic properties of a sand, *PhD thesis*, University of Southampton, UK.

Priest, J.A., Best, A.I. & Clayton, C.R. I., 2005. A laboratory investigation into the seismic velocities of methane gas hydrate-bearing sand, *J. geophys. Res.,* **110,** B04102, doi:04110.01029/02004JB003259.

Rad, N.S. & Tumay, M.T., 1987. Factors affecting sand specimen preparation by raining, *Geotechnical Testing Journal,* **10**(1), 31–37.

Rossi, G., Madrussani, G., Gei, D., Böhm, G. & Camerlenghi, A., 2005. Velocity and attenuation 3D tomography for gas-hydrates studies: the NW offshore Svalbard case., *Proc. Vth Int. Conf. gas hydrates*, Trondheim, Norway, **Paper 2040,** 677–682.

Salamatin, A.N. & Kuhs, W.F., 2002. Formation of porous gas hydrates, *Proc. Fourth Int. Conf. On Gas Hydrates*, Yokohama, Japan, 673–677.

Saxena, S.K., Avramidis, A.S. & Reddy, K.R., 1988. Dynamic moduli and damping ratios for cemented sands at low strains, *Can. Geotech. J.,* **25,** 353–368.

Sloan, E.D., Jr., 1998. *Clathrate hydrates of natural gases*, Marcel Dekker, New York.

Staykova, D.K., Hansen, T., Salamatin, A.N. & Kuhs, W.F., 2002. Kinetic diffraction experiments on the formation of porous gas hydrates, *Proc. Fourth Int. Conf. On Gas Hydrates*, Yokohama, Japan, 537–542.

Staykova, D.K., Kuhs, W.F., Salamatin, A.N. & Hansen, T., 2003. Formation of porous gas hydrates from ice powders: diffraction experiments and multistage model, *J. Phys. Chem. B,* **107,** 10 299–10 311.

Stern, L., Circone, S., Kirby, S.H. & Durham, W.B., 2005. SEM imaging of gas hydrate formation processes and growth textures, and comparison to natural hydrates of marine and permafrost origin, *Proc. Vth Int. Conf. gas hydrates*, Trondheim, Norway, **Paper 1046,** 300–310.

Stern, L.A., Kirby, S.H. & Durham, W.B., 1996. Peculiarities of methane clathrate hydrate formation and solid-state deformation, including possible superheating of water ice, *Science,* **273,** 1843–1848.

Strandenes, S. & Blangy, J.P., 1991. Ultrasonic velocity measurements in Troll sandstones, *Standford Rock Physics Proj.,* **47,** A1–A54.

Toksöz, M.N., Johnston, D.H. & Timur, A., 1979. Attenuation of seimic waves in dry and saturated rocks: 1. Laboratory measurements, *Geophysics,* **44**(4), 681–690.

Tsytovich, N.A., 1975. *The mechanics of frozen ground*, Mcgraw Hill, Washington, D.C.

Valiullin, R. & Furo, I., 2002. The morphology of coexisting liquid and frozen phases in porous material as revealed by exchange of nuclear spin magnetization followed by ^{1}H nuclear magnetic resonance, *J. Chem. Phys.,* **117,** 2307–2316.

Vanneste, M., Mienert, J., Guidard, S. & HYDRATECH-INGASS partners, 2002. 'Artic' gas hydrate provinces west of Svalbard, Norway, *Proc. Fourth Int. Conf. On Gas Hydrates*, Yokohama, Japan, 222–227.

Walter, J.E., Highter, W.H. & Vallee, R.P., 1982. Determining the maximum void ratio of uniform cohesionless soils, *Transportation Research Record 897,* 42–51.

Wang, Y.H., Cascante, G. & Santamarina, J.C., 2003. Resonant column testing: the inherent counter EMF effect, *Geotech. Testing. J.,* **26**(3), 342–352.

Winkler, K. & Nur, A., 1979. Pore fluids and seismic attenuation in rocks, *Geophys. Res. Lett.,* **6,** 1–4.

Winkler, K., Nur, A. & Gladwin, M., 1979. Friction and seismic attenuation on rocks, *Nature,* **277,** 528–531.

Wood, W.T., Holbrook, W.S. & Hoskins, H., 2000. In situ measurements of P-wave attenuation in methane hydrate and gas bearing sediments on the Blake Ridge, in *Proc. ODP. Results*, Vol. 164, pp. 265–272, eds Paull, C., Matsumoto, R., Wallace, P. & others, Ocean Drilling Program, College Station, Texas.